Published in final edited form as:
Lab Chip. 2010 June 21; 10(12): 1596–1603. doi:10.1039/b927316f.

Microdevice to capture colon crypts for *in vitro* studies

Yuli Wang[a], **Rahul Dhopeshwarkar**[a], **Rani Najdi**[b], **Marian Waterman**[b], **Christopher E. Sims**[a], and **Nancy Allbritton**[a,c]

[a] Department of Chemistry, University of North Carolina, Chapel Hill, NC 27599

[b] Department of Microbiology & Molecular Genetics, University of California, Irvine, California, 92697

[c] Joint Department of Biomedical Engineering, University of North Carolina, Chapel Hill, NC 27599 and North Carolina State University, Raleigh, NC 27695

Abstract

There is a need in biological research for tools designed to manipulate the environment surrounding microscopic regions of tissue. In the current work, a device for the oriented capture of an important and under-studied tissue, the colon crypt, has been designed and tested. The objective of this work is to create a BioMEMs device for biological assays of living colonic crypts. The end goal will be to subject the polarized tissue to user-controlled fluidic microenvironments in a manner that recapitulates the *in vivo* state. Crypt surrogates, polymeric structures of similar dimensions and shape to isolated colon crypts, were used in the initial design and testing of the device. Successful capture of crypt surrogates was accomplished on a simple device composed of an array of micron-scale capture sites that enabled individual structures to be captured with high efficiency (92 ± 3%) in an ordered and properly oriented fashion. The device was then evaluated using colon crypts isolated from a murine animal model. The capture efficiency attained using the fixed biologic sample was 37 ± 5% due to the increased variability of the colon crypts compared with the surrogate structures, yet 94% ± 3% of the captured crypts were properly oriented. A simple approach to plug the remaining capture sites in the array was performed using inert glass beads. Blockage of unfilled capture sites is an important feature to establish a chemical gradient across the arrayed crypts. A chemical concentration gradient ($C_{luminal}/C_{basal} > 10$) was demonstrated across the arrayed crypts for over 8 h. Finally unfixed colon crypts were demonstrated to be effectively captured by the micromesh array and to remain viable on the capture sites at 5 h after mouse sacrifice. The present study demonstrates the feasibility and potential for rationally microengineered technologies to address the specific needs of the biologic researcher.

Introduction

The ability to monitor and control the microenvironment of cells and tissues is one of the most promising applications for microengineered systems.1 Microfluidic devices have made it possible to easily and accurately modify the fluidic microenvironment of cells both temporally and spatially. For example, exposure of cells to chemotactic gradients in a quantitative manner can now be performed routinely through the use of microfluidic gradient makers.2, 3 Similarly, spatially discrete stimuli can be applied even to a portion of a single cell in order to study molecular responses at the subcellular level.4 While much of the effort to control the environment on the micron scale has been directed at single cells, many areas of biological research would benefit from devices designed to manipulate the

nlallbri@unc.edu; Fax: +1 (919) 962-2388; Tel: +1 (919) 966-2291.

environment surrounding microscopic regions of tissue. Such devices would enable biologists to more accurately recapitulate the stem cell niche, to influence the tumor microenvironment, and to manipulate inflammatory infiltrates, all of which are high priority areas of investigation.

Since many tissues are polarized with opposing sides exposed to different fluidic microenvironments, particularly intriguing is the potential for manipulating these environments in a discrete and independent manner. One area of research that would benefit from this selective control is the study of colon physiology in health and disease. The large intestine, or colon, is the last portion of the digestive system in most vertebrates.5 The principle functions of the colon are the re-absorption of salts and water and the elimination of undigested foodstuffs and other wastes.6 The surface of the colon is made up of a single layer of columnar epithelial cells, which form tube-like invaginations into the underlying connective tissue to form the basic functional unit of the colon, the crypt.7 The normal colon consists of millions of crypts with each crypt containing about 2,000 cells.8–10 The luminal face of the crypt is continually exposed to colonic contents and serves as a barrier to bacteria while simultaneously enabling absorption of water and electrolytes needed to maintain homeostasis. The opposing face of this epithelium lies adjacent to connective tissue and blood- or lymph-filled capillaries that serve to support the structural and metabolic needs of the colonic mucosa.

The colonic mucosa is one of the most vigorously self-renewing tissues of adult mammals. 11 The proliferative cells that serve to replenish the mucosa reside at the base of the crypts where stem cells give rise to progeny that terminally differentiate into colonic epithelial cells as they transit the crypt. Colon cancer, one of the most common cancers to afflict mankind, is thought to arise from the stem cell or its progeny, and study of the stem cell niche in the colonic crypt is an active area of research.7, 12, 13 Inflammatory bowel diseases, autoimmune diseases that include ulcerative colitis and Crohn's disease, cause significant human suffering.14 These diseases damage the colon through attack of crypt cells by inflammatory infiltrates. Due to technical challenges in the *in vitro* assessment of isolated crypts, studies of the various diseases involving colonic crypts have been restricted primarily to *in vivo* inspection and histological evaluation.7, 15 *In vivo* studies by endoscopy or noninvasive imaging enable examination of living colonic tissue at a macroscopic, but not cellular scale. Histologic evaluation of fixed tissue enables study at the cellular level, but the rich and dynamic qualities of the crypt tissue are lost.

There are many areas of investigation that would benefit from the ability to study the isolated colon crypt temporally while manipulating the environments of its luminal and basal sides. With the recent discovery of the colon stem cell marker *lgr5*, the impact of various environmental perturbations, including toxins or growth factors, on the stem cell niche could be directly studied.11, 16 The role of dietary components on crypt physiology could be readily tested, for example the loading of dietary calcium and its promotion of apoptosis as a mechanism for cancer prevention.17 Selective exposure of luminal and basal aspects of the crypt to chemotactic agents and other inflammatory mediators would facilitate the study of the interplay of inflammation and colonic epithelium in real time. With recent advances in the long-term culture of isolated colon crypts from mouse model systems, technologies to enable controlled, in-depth studies of this tissue are needed.12, 18 In the current study, the preliminary work to build a microdevice for the *in vitro* study of isolated mouse colon crypts at the interface of two different environments is presented. Several difficulties have been overcome to address the task of capturing isolated three-dimensional structures in a selective orientation that will allow the luminal and basal sides of the crypts to be differentially exposed. Microdevices to capture isolated tissue possessing a complex

shape for *in vitro* study, such as that presented here, have enormous potential in future biomedical research.

Materials and Methods

Materials

SU-8 photoresist (formulation 10) was purchased from MicroChem Corp. (Newton, MA). The Sylgard 184 silicone elastomer kit was purchased from Dow Corning (Midland MI). Gamma-butyrolactone, propylene glycol monomethyl ether acetate, toluidine blue, Corning glass slide (75 mm × 50 mm × 1 mm), triarylsulfonium hexafluoroantimonate salts (mixed, 50 wt. % in propylene carbonate), glass beads (size 75 μm, acid-washed) were obtained from Sigma-Aldrich (St. Louis, MO). 1,1′-Dioctadecyl-3,3,′,′-tetramethylindocarbocyanine perchlorate (DiI), Oregon Green 488 carboxylic acid diacetate, dithiothreitol (DTT), ethylenediaminetetraacetic acid (EDTA, 0.5 M, pH 8.0), Ca^{2+}/Mg^{2+}-free Hanks' Balanced Salt Solution (HBSS) were obtained from Invitrogen (Carlsbad, CA). EPON epoxy resin 1002F (fusion solids) was purchased from Miller Stephenson Chemical Co. (Sylmar, CA). Biologic buffers and other regents were obtained from Fisher Scientific (Fairlawn, NJ).

Formulation of 1002F photoresist

1002F photoresist was formulated by mixing 1002F resin, photoinitiator (triarylsulfonium hexafluoroantimonate salts), and solvent (gamma-butyrolactone) as previously described.19 The weight ratio of resin:photoinitiator:solvent was 49:4.9:46.1 for formulation 10 (which generates 10 μm thickness of film at the spin speed of 2000 rpm), 61:6.1:32.9 for formulation 50, and 65:6.5:28.5 for formulation 100. The components were placed in a 500 mL brown glass bottle and the mixture was mixed by slowly rotating the bottle on a roller system (Wheaton Science Products, Millville, NJ) until the resin was fully solubilized.

Colon crypt isolation and dye staining

Normal colon tissue, obtained from mice (129Sv/C57BL/6 strain), was rinsed 5 times with 20 mL HBSS. The tissue was then incubated in 1mM EDTA and 0.5 mM DTT in HBSS for 60–90 min to dissolve the surface mucosa. The tissue was rinsed 3 times with 20 mL PBS in a 50 mL conical tube. 30 mL PBS was placed in the tube and it was then shaken vigorously for 5 seconds. The detached crypts were then collected for immediate use, or fixed in 3.7% formaldehyde in PBS and stored at 4 °C.

To image the crypts by epifluorescence microscopy, the crypts were stained with DiI, an orange-red fluorescent dye. A stock solution of DiI was made by dissolving DiI in 100% ethanol at 0.5 mg/ml. For staining, 100 μL of the DiI stock solution was added to 500 μL of colon crypt suspension in PBS (~50,000 crypts/mL), and the suspension was incubated at ambient temperature for 60 min on a rotary shaker (Labquake, Barnstead/Thermolyne, Dubuque, Iowa). After the incubation, the suspension was transferred to a centrifuge tube, diluted with 10 mL PBS buffer, and centrifuged at 2000 rpm for 1 min. The supernate was decanted and the pellet composed of the stained crypts was re-suspended in 10 mL PBS buffer.

Fabrication of crypt surrogates

Figure 1A is a schematic of the fabrication process to create the crypt surrogates. A glass slide was cleaned with deionized water and ethanol, and then dried with a stream of nitrogen (Fig. 1A–i). A 1002F film of 150-μm thickness was obtained by spin-coating 1002F photoresist (formulation 100) on the glass slide at 500 rpm for 10 s followed by 1500 rpm for 30 s on a WS-200-4NPP spin coater (Laurell Technologies Corp.) (Fig. 1A–ii). The coated slide was baked in a convection oven at 95 °C for 60 min. After cooling to room

temperature, an SU-8 film of 10-μm thickness was spin-coated on the top of 1002F film using SU-8 photoresist (formulation 10) at 500 rpm for 10 s followed by 2000 rpm for 30 s (Fig. 1A–iii). The slide was baked in a 95 °C oven for 5 min. The film was then exposed to UV light at a dose of 2000 mJ/cm^2 through a photomask using an Oriel collimated UV source equipped with a 350 nm short pass filter (PL-360-LP, Omega Optical, Brattleboro, VT) (Fig. 1A–iv). The post-exposure baking was performed in a 95 °C oven for 16 min. The sample was then developed in propylene glycol monomethyl ether acetate for 15 min, rinsed with 2-propanol, and dried by a stream of nitrogen (Fig. 1A–v). To prevent the aggregation of surrogates in water, the sample was treated with air plasma for 5 min using a plasma cleaner (Harrick Plasma, Ithaca, NY). The structures were detached from the glass slide by scraping using a single-edge razor blade, and then rinsed into a 50-mL centrifuge tube using phosphate buffered saline (PBS). Since 10,000 surrogate structures were fabricated on a 20 mm × 20 mm area, a concentration of 400 surrogates/mL was obtained by suspending the detached structures in 25 mL of PBS buffer.

Fabrication of an array of micromesh

Figure 2A shows the schematic of the fabrication process for a micromesh array. A film of 1002F of 50-μm thickness was produced by spin-coating 1002F photoresist (formulation 50) on a glass slide at 2000 rpm (Fig. 2A–ii). After baking at 95 °C for 40 min, the film was exposed to UV light at a dose of 800 mJ/cm^2 (Fig. 2A–iii). The post-exposure baking was performed in a 95 °C oven for 10 min. The sample was then developed for 8 min, and baked on a 120 °C hotplate for 60 min (Fig. 2A–iv). Finally, the freestanding film was released from the glass slide by soaking the sample overnight in a soap solution (Fig. 2A–v). A 20 × 20 array of capture sites was used for all experiments described.

Loading of colon crypts on the microdevice

Figure 3 shows a schematic of loading crypts on the micromesh arrays. The freestanding film was glued to a polypropylene tubing (ID = 15 mm, OD = 19 mm, length = 40 mm) using PDMS prepolymer (10:1 mixture of base:curing-agent of Sylgard 184 kit) (Fig. 3A). The PDMS was cured in a 75 °C oven for 60 min. The film was made hydrophilic by treating it with an air plasma for 5 min. The tubing was then placed in a petri dish (diameter × height = 55 mm × 14 mm). A specified number of crypts (see “Results”) were suspended in 50 mL PBS buffer. The crypt suspension was added to the tubing and flowed by gravity through the film where the crypts were captured by the capture sites in the micromesh array (Fig. 3B). During loading, the liquid height was maintained at about 29 mm above the film by adding PBS to the tubing. Excess liquid was removed from the petri dish during loading. The microscope stage holding the device was gently tapped with a finger at ~ 1 Hz during the loading procedure to aid in the alignment of the crypts during capture. After loading, unfilled capture sites were plugged by settling glass beads in suspension (400 beads/mL) onto the array (Fig. 3C).

Live crypts were loaded to the micromesh arrays immediately after the crypts were isolated from colon (within 3 h of mouse sacrifice). To test the viability of the captured crypts, 1 mL of Oregon green 488 carboxylic diacetate (20 μM) in PBS was added to the tubing (Fig. 3D). After 10 min, the captured crypts were washed by 20 mL PBS to remove Oregon green diacetate. The crypts were then examined on an inverted fluorescence microscope (excitation/emission 470 nm/535 nm).

Measurement of dye movement across a crypt array

Toluidine blue (1% in PBS, 30 μL) was added to the luminal side (total volume 1 mL) of an array. At varying times, 120 μL was removed out from basal side (total volume 19 mL). The optical absorption (633 nm) of 100 μL of the liquid samples was measured using a

SpectraMax M5 microplate reader (Molecular Devices, Sunnyvale, CA). The concentration of toluidine blue on the basal side (C_{basal}) was then obtained from the optical density. The concentration on the luminal side ($C_{luminal}$) was calculated from C_{basal}, the total amount of dye, and the liquid volumes of the luminal and basal reservoirs. Measurements were performed on three separate samples to obtain an average toluidine blue concentration.

Optical micrographs

The samples were imaged under brightfield or standard epifluorescence microscopy using an inverted microscope (Nikon TE2000-U). A fluorescein filter set (excitation/emission 470/535) was used for surrogate crypts and Oregon green diacetate stained crypts, while a rhodamine filter set (excitation/emission 540/625) was used for the crypts stained with DiI. Differential interference contrast (DIC) images were obtained using with a Leica SP2 microscope.

Scanning electron micrograph

To image colon crypts using scanning electron microscopy (SEM), the suspension was desalted as follows: 100 μL of fixed colon crypts (in PBS) was added to 10 mL distilled water and centrifuged at 2000 rpm for 1 min. The supernate was decanted and the crypts were then re-suspended in 10 mL distilled water. 100 μL of this suspension was then added to a cover slip, and the sample was dried under ambient conditions. For the crypts captured on the microdevices, salts were removed by a final rinse of DI water through the microdevices. The various dried samples were coated with a 6-nm thick gold layer using a sputter coater and imaged by SEM (FEI Quanta 200 ESEM, FEI Company).

Results and Discussion

Description of colon crypts and surrogates

Isolated colon crypts have a unique mushroom-shaped geometry. Generally the diameter of the luminal (or apical) end is larger than that of the basal (or blind) end.20 Figure 1D shows a micrograph of a typical colon crypt suspended in PBS, together with the debris of epithelial cells or disrupted crypts. The isolated crypts displayed a wide size distribution with a length of 241 ± 49 μm, a diameter at the luminal end of 100 ± 23 μm, and a diameter at the basal end of 58 ± 10 μm (n = 20 crypts). Crypts stained with DiI were imaged under fluorescence and DIC (Fig. 1D inset). The mushroom-shaped geometry of the crypt was clearly demonstrated in the SEM image (Fig. 1E). It should be noted that shrinkage of the imaged crypt occurred as a result of drying under the conditions used for SEM imaging.

Due to the limited availability of isolated colon crypts, a surrogate model was created for the initial testing of the microdevices. Figure 1A shows a simple process to fabricate the surrogate crypts. Two layers of photoresists were sequentially spin coated on a glass slide. The bottom layer (1002F of 150-μm thickness) was less photosensitive than the top layer (SU-8 of 10-μm thickness). For photoresists of the same thickness, the UV dose generally required for 1002F was 2–4 times higher than that for SU-8.19, 21 The two-layer film was exposed to UV through a mask at a dose of 2000 mJ/cm^2, which was 8-fold over-exposure for the 10-μm SU-8 layer, and 2-fold over-exposure for the 150-μm 1002F layer. As a result of the 4-fold greater exposure for the top layer of SU-8 compared to the 1002F layer in the UV-exposed portion, the top layer was larger in diameter than the bottom layer resulting in a mushroom-shaped structure (Fig. 1B and 1C) similar to the crypts. Although the opening on the photomask was 40 μm, the UV overexposure caused the diameter of surrogates to be 91 ± 6 μm for the top layer, and 54 ± 3 μm (n = 20 structures) for the bottom layer. The length was 155 ± 7 μm. Compared with the isolated crypts the surrogates had greater uniformity and geometry. The size of surrogates could be adjusted by fabrication conditions such as

spin-coating speed, UV-exposure dose and photomask design. It is noted that the surrogates were fluorescent when using a fluorescein-filter set because the SU-8 layer has 5–10 times higher autofluorescence than the bottom 1002F layer (Fig. 1B inset).19 In addition, surrogates to mimic the debris (ruptured crypts and clumps of dissociated cells) seen in suspensions of the isolated crypts were created. The debris surrogates were composed of a mixture of rectangular particles of 60 μm × 60 μm × 30 μm and 40 μm × 40 μm × 30 μm (Fig. 1B) fabricated by exposing a 30-μm thick SU-8 photoresist to UV light through a mask with 60 μm × 60 μm and 40 μm × 40 μm openings.

Fabrication of microstrainer and micromesh arrays

To determine whether an array of colon crypts could be assembled, two different support structures were fabricated, a microstrainer array and a micromesh. An array of microstrainers was fabricated according to the process outlined in Fig. S1. Micromesh, a simpler microdevice than the microstrainer, was fabricated according to the process outlined in Fig. 2A. A freestanding film made from the commercial photoresist SU-8 was too brittle to be used in the manipulation steps depicted in Fig. 3, which included film detachment from a glass substrate as well as attachment of tubing to the final film. An alternative photoresist 1002F was more pliable than SU-8 and thus could withstand the manipulation steps of the developed film.19 By soaking in a soap solution for 16 h, the film could be detached from the glass as a freestanding structure. The detached film remained highly transparent. The micromesh arrays were composed simply of circular holes. Arrays were created using a variety of diameters (40–150 μm) for the openings. Figures 2B and 2C show SEM images of a portion of a micromesh array composed of 80-μm capture sites. The freestanding micromesh film made from 1002F was found to be resilient and did not fracture even after bending and folding.

Loading colon crypts and surrogates onto the microstrainer and micromesh arrays

The freestanding film composed of the microstrainer or micromesh array was glued to a polypropylene tube that served as a fluid reservoir (Fig. 3A). The assembly was then treated with an air plasma to make the surface of the film hydrophilic. This was necessary to prevent air entrapment in the openings of the microstrainer or micromesh. Adding a suspension of crypts or surrogates to the tubing reservoir resulted in fluid flow through the openings in the film (Fig. 3B) that carried the suspended structures through the openings where they were captured. The microstrainer was initially tested using crypt surrogates mixed with debris surrogates. This structure captured the crypt surrogates, but capture sites were frequently blocked by the debris surrogates (Fig. S2A), thus making individual sites unavailable for capture. When the microstrainer was used to capture actual crypts, many of the microstrainer capture sites were blocked by the epithelial debris present in the suspension rather than captured crypts (Fig. S2B).

The simpler structure of the micromesh was then tested. The rationale for the micromesh design was based on the geometry of the crypts. The smaller basal end of the crypt was expected to enter the site under the influence of the fluid flow. In contrast, the larger luminal end would prevent the crypt from entering the capture site luminal end first, and would also act to retain a crypt that entered the site basal end first. The debris, which was generally much smaller than the crypts, was expected to flow through the holes without being retained. It was found in testing with surrogates (crypt and debris) that this was indeed the case. Figures 4A and 4B show a portion of the micromesh array composed of 70-μm capture sites before and after loading with surrogates. After loading with surrogates, 92 ± 3% of the sites (n = 5 independent experiments) had captured surrogate crypts. No capture sites were found to have been blocked by the surrogate debris. The surrogate loaded micromesh was imaged by SEM on both faces (Fig. 4C and 4D). The SEM images demonstrated the capture

of surrogate crypts by the capture sites with the luminal end hanging over the site on the upper side of the film (Fig. 4C), while the basal end dangled out of the hole on the underside of the film (Fig. 4D).

Since the micromesh was shown to effectively capture the surrogates, actual crypts were then tested with this device. A suspension of fixed crypts was loaded on a device composed of an array of 80-μm capture sites in the same manner as described above. Imaging by brightfield and DIC suggested that the crypts were oriented vertically within the holes with the basal end extending below the lower face of the array substrate (Fig. 4E, F). The orientation of the crypts captured by the micromesh array was clearly shown by SEM analysis of both faces of the film after crypt capture (Fig. 4G–J). Although the captured crypts shrank due to vacuum drying of the sample for the SEM imaging, they remained in their captured positions. The luminal end was shown to be trapped on the upper side of the film, while the basal end extended out of the lower face of the film.

Gentle tapping of the device with a finger during the loading process was found to be important for properly orienting the crypts during capture. To be captured, the crypts must be aligned with the fluid streamlines (Fig. S3A) such that the basal end flows into the capture site ahead of the luminal end. When the crypts were settled on the micromesh in the absence of vibration, only 12% ± 5% (n = 4 experiments) of capture sites were observed to contain crypts in the proper orientation. Most of the crypts were oriented either horizontally (crypts aligned perpendicular to the capture sites as shown in Fig. S3B or with the luminal end in the capture site, but the basal end pointing upwards. In both of these orientations, the crypt's dimensions (150–250 μm length or ~100 μm luminal end) in comparison to the smaller (~70 μm) mesh openings prevented the crypts from being properly captured in the micromesh. It was found that vibration created by gently tapping the microscope stage that held the device re-oriented un-captured crypts along the fluid flow with their basal ends pointing toward the capture sites. In these studies, 94% ± 3% (n = 3 experiments) of captured crypts were properly oriented. It should be noted that if the vibration was too forceful, crypts that were already captured could be displaced from their capture sites, thus reducing loading efficiency.

Loading efficiency of crypt surrogates and plugging of open capture sites

To determine the loading efficiency, a suspension of crypt surrogates (400 surrogates in 50 mL PBS) was added to a micromesh array composed of 20 × 20 capture sites. The estimated number of surrogates (400) used was equal to the number of capture sites making up the array. In these studies, the loading efficiency was defined as the percentage of sites that successfully captured the surrogates as verified by microscopic imaging. Gentle tapping as described above was used to achieve the maximal loading efficiency. The loading efficiency of crypt surrogates depended on the diameter of the capture sites, as illustrated in Figure 5A. The optimal loading efficiency for surrogates was 92 ± 3% (n = 5) when an array of 70-μm sites was used. Figure 5B shows an 8 × 10 portion of an array of 70-μm sites in which 76 sites captured crypt surrogates, and only 4 remained empty. A typical surrogate possessed a diameter of 92-μm at the luminal end, and 53-μm at the basal end (Fig. 5A inset). The loading efficiency was reduced when the diameter of the capture site was less than 70 μm or greater than 90 μm. Not surprisingly, these data show that in order to capture the surrogate the size of the site must be greater than the basal end and smaller than the luminal end of the surrogate.

Although a high loading efficiency could be achieved for crypt surrogates, some sites remained empty. Since the eventual goal will be to perform assays that expose captured crypts to two different fluidic microenvironments on opposite sides of the array, the empty sites must be plugged or sealed in order to prevent fluid exchange across the array. A simple

way to plug these holes was found using physiologically inert glass beads of slightly larger diameter than the capture sites in the array. A suspension of glass beads (100 beads in 1 mL PBS, average diameter 75 μm) was added, and the beads loaded in the same manner as crypts. Brightfield (Fig. 5D, E) and SEM images (Fig. 4C, D) showed the empty capture sites firmly plugged by the glass beads. An excess number of glass beads were added to ensure all capture sites that lacked crypts were plugged. The previously captured crypt surrogates remained in place during the plugging procedure.

Loading efficiency of fixed crypts and plugging of open capture sites

The loading efficiency of the isolated crypts was tested using a suspension of fixed crypts (400 crypts in 50 mL PBS) added to a micromesh array in a manner identical to that described in the previous section. The capture efficiency was 37 ± 5% (n = 5) for the crypts when an array composed of 80-μm sites was used. It is likely that the greater size distribution of the actual colon crypts as compared to the surrogates lowered the likelihood of their capture compared to that of the surrogates. As with the surrogates, the loading efficiency of the crypts depended on the diameter of the capture sites (Fig. 6A). Shown in Figure 6B is a 6 × 8 portion of an array of 80-μm sites in which 28 sites held captured crypts. A fluorescence image (Fig. 6C) of crypts stained with DiI clearly showed the location of captured crypts. A typical crypt had a diameter of 113-μm at the luminal end, and a diameter of 54-μm at the basal end (Fig. 6A, inset). A capture site diameter between 80 – 90 μm was found to provide the highest capture efficiency. Open sites could be plugged by adding a suspension of glass beads (Fig. 6D, E) after the crypt capture procedure as described in the previous section. Colon crypts have a relatively wide distribution in size, for example, diameter of basal end is 58 ± 10 μm. This indicates that crypts of a certain size are preferentially captured in the device. To capture crypts of different size, an array of holes with a size distribution corresponding to that of the colon crypts could be utilized.

Formation of a gradient across the crypt array

Formation of chemical gradients across the crypts is thought to be critical for proper colon development and differentiation. For example, a gradient of gremlin (expressed by the myofibroblasts underlying the intestinal epithelium) across the crypts is thought to be necessary for maintaining Wnt signaling in the stem cell compartment at the base of every crypt.22 To determine whether the crypt array could support a molecular gradient between the luminal and basal crypt sides, toluidine blue was added to the luminal side of the array (Fig 3D). Movement of toluidine blue was followed over time by measuring the absorbance of the dye on the basal side (Fig S4). A molecular gradient of toluidine blue ($C_{luminal}/C_{basal}$ >10) was formed that lasted over 8 hours, the longest time measured (Fig. 7A). Thus chemical gradients can be formed across the crypt arrays and may be useful in the study of crypt differentiation and polarization.

Capturing living colon crypts in the micromesh array

A long term goal for the current device is the formation of living crypt arrays for biomedical experimentation. Since living crypts are softer and more flexible relative to fixed crypts, it was important to assess whether they could be efficiently loaded into the arrays in a viable state. To demonstrate whether living crypts could be arrayed in the micromesh array, freshly isolated colon crypts were added to an array (400 capture sites, 80 μm holes). When 1,500 crypts were loaded onto the array, 80% of the capture sites were filled with crypts. Fig. 8A shows 58 crypts captured in a 72-site segment. To determine whether the crypts remained viable after placement on the array, Oregon green diacetate (a viability dye) was added to the crypt array. All of the crypts loaded into the array actively metabolized the viability dye to its fluorescent form (Oregon green) and concentrated the dye within the cellular cytoplasm (Fig. 8B and C). This data suggests that an array of living crypts was formed.

Conclusions

Isolated colon crypts were captured in an oriented fashion on a simple device composed of an array of micron-scale capture sites. It was found that a capture site composed of a simple circular opening, termed a micromesh had several advantages for capturing the crypts over an array composed of microstrainers. The micromesh was simple to create needing only a one-step fabrication process. In actual use, the micromesh allowed debris to pass freely through the capture site while the microstrainer frequently became clogged. To improve the capture efficiency and orientation the isolated crypts were loaded onto the device as a suspension and settled onto the array under the influence of fluid flow while a low frequency vibration was applied. It is likely that the capture efficiency could be further improved by sorting the crypts according to size before loading them on to the micromesh. The results in the present study show the feasibility of using the micromesh to capture and form an array of living colon crypts. A future goal is to load the crypts into an array within a microfluidic device so that the luminal and basal sides can be accessed by distinct aqueous environments. Such a device will facilitate in vitro studies of ion transport, stem cell differentiation and other aspects of crypt physiology.

Acknowledgments

We thank Robert Edwards (Department of Pathology, UCI) for providing the murine colons for experiments with fixed crypts and for advice on crypt isolation and preparation. We also acknowledge Christopher Dekaney (Department of Surgery, UNC) for providing murine colons for experiments with living crypts. This research was supported by NIH (R01 EB007612 and R01 EB004436).

References

1. Sims CE, Allbritton NL. Lab Chip. 2007; 7:423–440. [PubMed: 17389958]
2. Keenan TM, Folch A. Lab Chip. 2008; 8:34–57. [PubMed: 18094760]
3. Paguirigan AL, Beebe DJ. Bioessays. 2008; 30:811–821. [PubMed: 18693260]
4. Sawano A, Takayama S, Matsuda M, Miyawaki A. Dev Cell. 2002; 3:245–257. [PubMed: 12194855]
5. Campbell, NA.; Reece, JB.; Taylor, MR.; Simon, EJ.; Dickey, JL. Biology: Concepts & Connections. Vol. Chapter 21. Benjamin Cummings; San Francisco, CA: 2009.
6. Henrikson, RC.; Kaye, GI.; Mazurkiewicz, JE. Histology. Williams & Wilkins; Baltimore, MD, Baltimore, MD:
7. Humphries A, Wright NA. Nature Reviews Cancer. 2008; 8:415–424.
8. Cheng H, Bjerknes M, Amar J. Gastroenterology. 1984; 86:78–85. [PubMed: 6689675]
9. Kim KM, Shibata D. Oncogene. 2002; 21:5441–5449. [PubMed: 12154406]
10. Potten CS, Loeffler M. Development. 1990; 110:1001–1020. [PubMed: 2100251]
11. van der Flier LG, Clevers H. Annu Rev Physiol. 2009; 71:241–260. [PubMed: 18808327]
12. Sato T, Vries RG, Snippert HJ, van de Wetering M, Barker N, Stange DE, van Es JH, Abo A, Kujala P, Peters PJ, Clevers H. Nature. 2009; 459:262–U147. [PubMed: 19329995]
13. Garrison AP, Helmrath MA, Dekaney CM. J Pediatr Gastroenterol Nutr. 2009; 49:2–7. [PubMed: 19502994]
14. Yantiss RK, Odze RD. Histopathology. 2006; 48:116–132. [PubMed: 16405661]
15. Takayama T, Miyanishi K, Hayashi T, Kukitsu T, Takanashi K, Ishiwatari H, Kogawa T, Abe T. Clinical Gastroenterology and Hepatology. 2005; 3:S42–S45. [PubMed: 16012995]
16. Barker N, van Es JH, Kuipers J, Kujala P, van den Born M, Cozijnsen M, Haegebarth A, Korving J, Begthel H, Peters PJ, Clevers H. Nature. 2007; 449:1003–U1001. [PubMed: 17934449]
17. Whitfield JF. Cancer Lett. 2009; 275:9–16. [PubMed: 18725175]
18. Ootani A, Li XN, Sangiorgi E, Ho QT, Ueno H, Toda S, Sugihara H, Fujimoto K, Weissman IL, Capecchi MR, Kuo CJ. Nat Med. 2009; 15:1–U140. [PubMed: 19129764]

19. Pai JH, Wang Y, Salazar GT, Sims CE, Bachman M, Li GP, Allbritton NL. Anal Chem. 2007; 79:8774–8780. [PubMed: 17949059]

20. Singh SK, Binder HJ, Geibel JP, Boron WF. Proc Natl Acad Sci U S A. 1995; 92:11573–11577. [PubMed: 8524806]

21. Datasheet, T. SU-8 Photoresist Formulations. http://www.microchem.com/products/su_eight.htm

22. Kosinski C, Li VSW, Chan ASY, Zhang J, Ho C, Tsui WY, Chan TL, Mifflin RC, Powell DW, Yuen ST, Leung SY, Chen X. Proc Natl Acad Sci U S A. 2007; 104:15418–15423. [PubMed: 17881565]

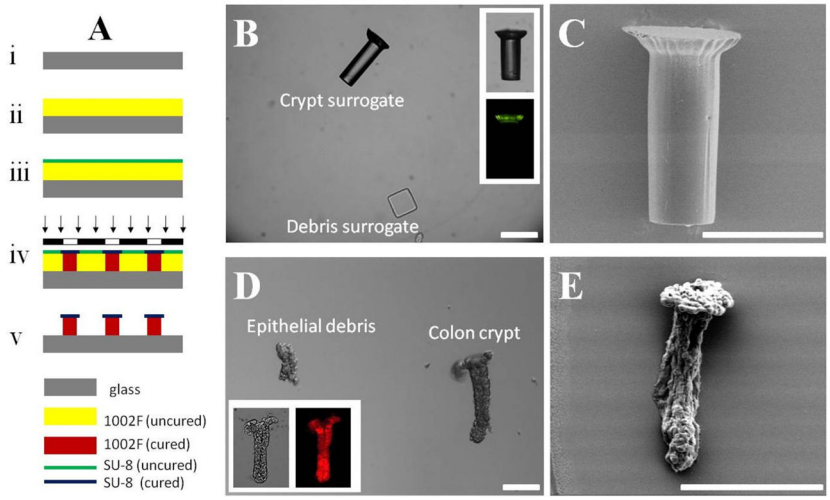

Fig. 1.

Surrogate crypts and colonic crypts (with debris). (A) Schematic of the fabrication process for the crypt surrogate. (B) Brightfield and fluorescence (inset) images of crypt surrogate. Debris surrogate is also shown. (C) SEM image of crypt surrogate. (D) DIC and brightfield/ fluorescence (inset) images of isolated colon crypts. Typical epithelial debris is also shown. (E) SEM image of colon crypt. Scale bar is 50 μm.

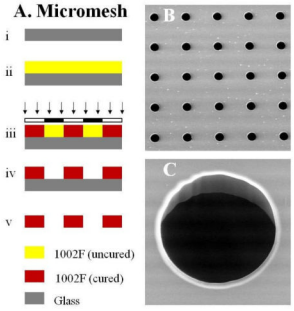

Fig. 2.

Micromesh array. (A) Schematic of the fabrication process for the micromesh. (B) and (C) SEM images of the micromesh. The diameter of capture sites in the micromesh was 80 μm.

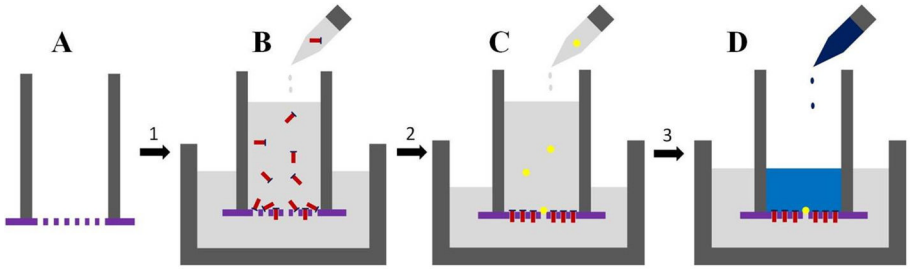

Fig. 3.

Schematic of protocol for capturing colon crypts and for formation of a basal-luminal chemical gradient. (A) A freestanding array of micromesh was glued to polypropylene tubing. (B) A suspension of colon crypts was added so that the luminal side of the crypt was contiguous with the lumen of the polypropylene tube. The crypt basal side was facing the lower, larger reservoir. (C) A suspension of glass beads was added. (D) A gradient was formed across the crypt array by adding a chemical to the luminal side.

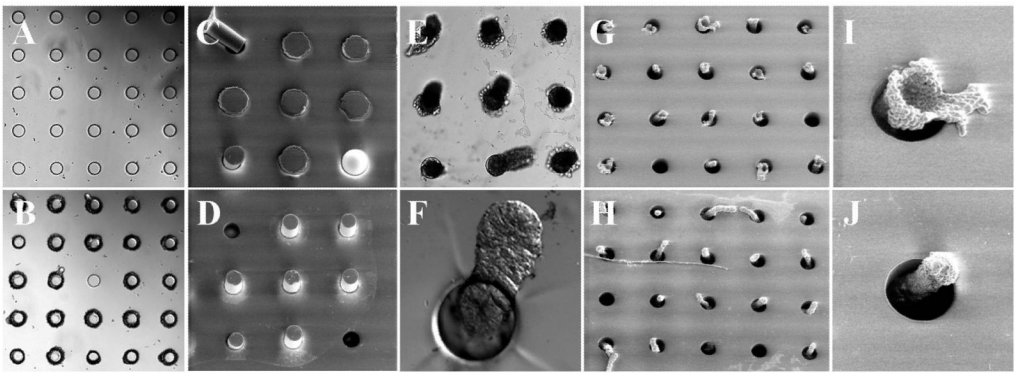

Fig. 4.

Loading surrogates or colon crypts into the micromesh. (A–D) Loading of surrogates into a micromesh array (diameter of opening = 70 μm). Brightfield images of a micromesh array before (A) and after (B) loading with surrogates. SEM images of a loaded micromesh array viewed from top (C) and bottom (D) sides. (E–J) Loading of isolated colon crypts on a micromesh array (diameter of opening = 80 μm). (E) Brightfield image of a micromesh array after loading. The crypts were found captured in the device oriented vertically and so they appear dark due to blockage of light by the crypt tissue. (F) DIC image showing a dangling crypt in a capture site viewed from the bottom face. (G–J) SEM images of a micromesh array loaded with crypts viewed from top (G, I) and bottom (H, J). (I) and (J) are close-up images of individual capture sites in “G” and “H”, respectively.

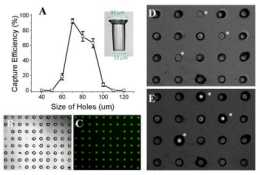

Fig. 5.

Efficiency of loading crypt surrogates in the micromesh array. (A) Efficiency of loading crypt surrogates *vs.* capture site diameter. The inset image shows the surrogate's dimensions. (B) Brightfield image showing the loading on an 8 × 10 portion of an array of 70-μm capture sites. (C) Fluorescence image of "B" taking advantage of the autofluorescence of the surrogates to clearly show the location of captured surrogates. (D–E) Brightfield images of the upper (D) and lower (E) faces of the array with captured surrogates. Unfilled capture sites (marked with an asterisk) were plugged with 75- μm glass beads.

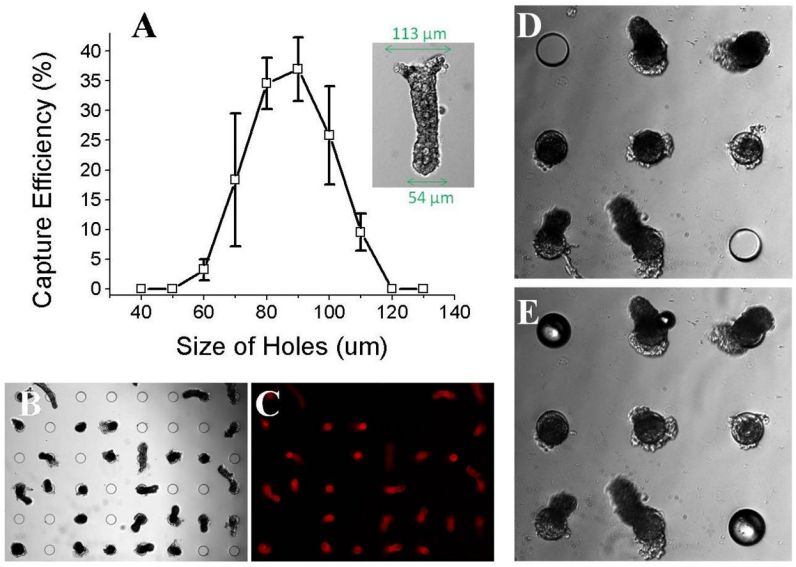

Fig. 6.

Efficiency of loading isolated colon crypts in the micromesh array. (A) Efficiency of loading crypts *vs.* capture site diameter. The inset image shows the dimensions of a typical crypt. (B) Brightfield image showing a 6 × 8 portion of an array of 80-µm capture sites. (C) Fluorescence image of "B". (D–E) Brightfield images of the array with captured crypts before (D) and after (E) unfilled capture sites were plugged with 75- µm glass beads.

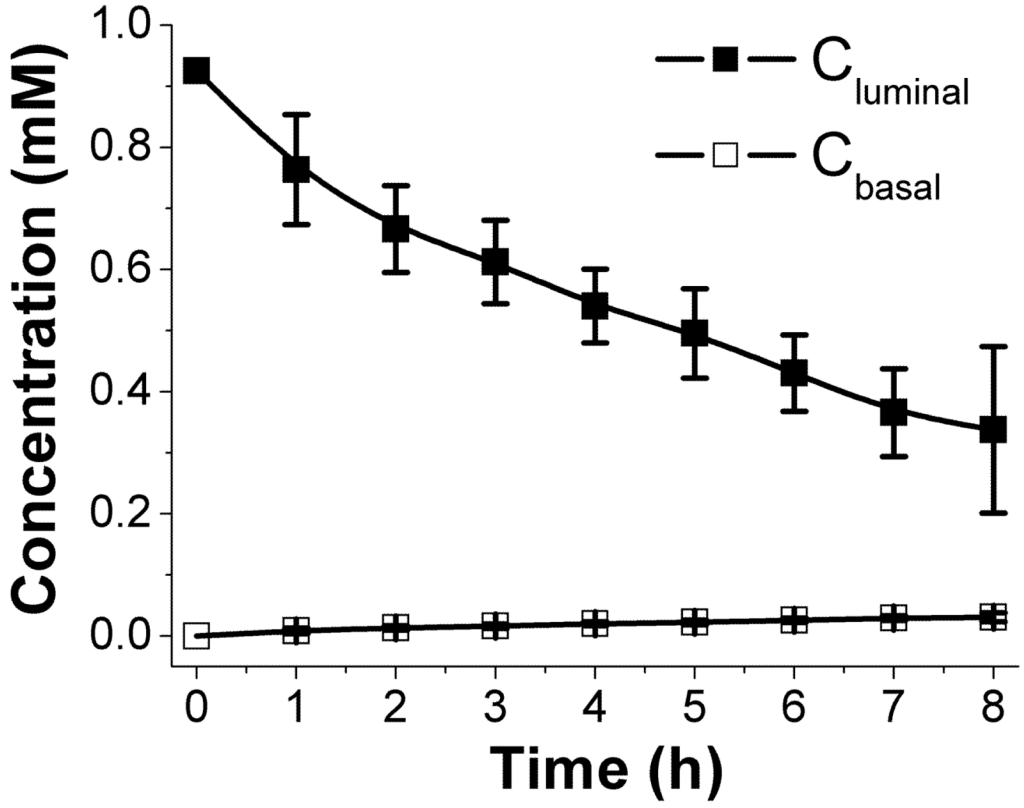

Fig. 7.

Formation of a toluidine blue gradient across the crypt array. Shown is the concentration of toluidine blue on the luminal side ($C_{luminal}$) and basal side (C_{basal}) *vs.* incubation time.

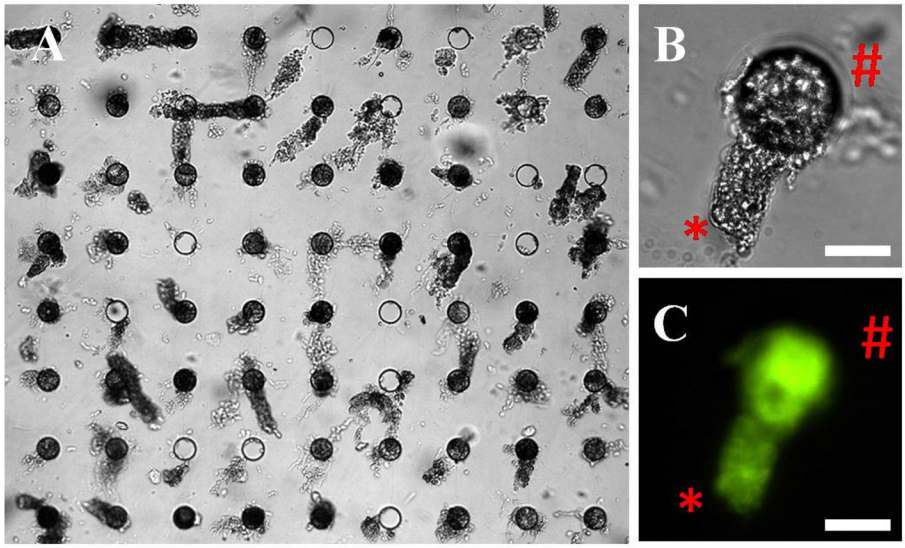

Fig. 8.

Loading live colon crypts on the micromesh. (A) Brightfield image of a micromesh array after loading with live crypts (80 μm sites). (B) A close-up brightfield image showing a dangling crypt in a capture site: basal end (*) and luminal end (#). (C) Fluorescence image of the same crypt stained with Oregon Green 488 carboxylic acid diacetate. Scale bar is 50 μm for (B) and (C).